

pubs.acs.org/acscatalysis Research Article

# Transient and Steady-State Kinetic Studies of Formaldehyde Alkylation of Benzene to Form Diphenylmethane on HZSM-5 Catalysts

Brandon L. Foley and Aditya Bhan\*



Cite This: ACS Catal. 2020, 10, 10436-10448



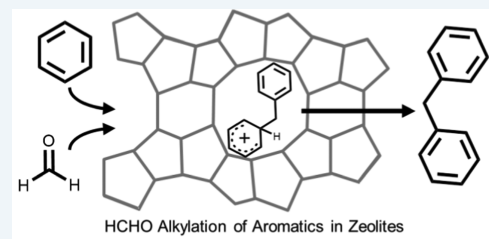
ACCESS

Metrics & More

Article Recommendations

Supporting Information

ABSTRACT: A combined steady-state and transient kinetic study on the mechanism of diphenylmethane (DPM) formation in HZSM-5 from HCHO and benzene revealed two kinetically relevant steps—the alkylation of benzene by HCHO and the deprotonation of a diphenylmethane benzenium ion (DPM<sup>+</sup>) to form DPM. The functional dependence of the rate of each of these reactions was determined by observing the transient rate after a step-change in reactant partial pressures, specifically whether the rate was discontinuous through a step-change in partial pressure. Steady-state isotopic switching experiments revealed that a persistent surface intermediate with two aromatic rings, likely DPM<sup>+</sup>, is formed and has a fractional coverage ranging from sparse (near-zero) to complete (near-



Transient and Steady-State Rates ⇒ Mechanism ⇒ Kinetic Model

one) that varies with process conditions. Reaction orders obtained from steady-state rate measurements suggest that HCHO,  $C_6H_6$ , and  $H_2O$  competitively adsorb on acid sites and that DPM<sup>+</sup> deprotonation is first-order in  $C_6H_6$ , implying that deprotonation is assisted by the presence of aromatics. Herein, we propose a complete mechanism for the condensation between HCHO and  $C_6H_6$  to form DPM, and from this mechanism, a six-parameter (three kinetic/thermodynamic parameters, three apparent activation/thermodynamic energies) kinetic model is derived that quantitatively describes the transient and steady-state rates and steady-state fractional coverages of DPM<sup>+</sup>.

KEYWORDS: chemical transients, alkylation, SSITKA, formaldehyde, kinetic modeling, methanol-to-hydrocarbons conversion, catalyst deactivation

#### 1. INTRODUCTION

Formaldehyde, formed by hydrogen transfer from methanol, is implicated as being potent in mediating the transformation of active hydrocarbon pool species (olefins and aromatics) to inactive polycyclic hydrocarbons during methanol-to-hydrocarbons (MTH) catalysis on microporous solid acid zeolite/ zeotype catalysts.<sup>1-4</sup> Formaldehyde reacts with unsaturated hydrocarbons via sequential alkylation and dehydration reactions  $C_nH_x + HCHO \rightarrow C_{n+1}H_x + H_2O$ , resulting in the addition of one degree of unsaturation to hydrocarbon pool chain carriers, which shifts product selectivity and induces catalyst deactivation in microporous zeolite/zeotype materials. 1,5,6 Formaldehyde can react with any unsaturated hydrocarbon species during methanol-to-hydrocarbon catalysis, including olefins, dienes, and aromatics. Investigation of the mechanism and kinetics of each of these reactions is important for determining the relative contribution of each pathway to the consumption of HCHO and for elucidating deactivation mechanisms during MTH catalysis. Herein, we investigate the kinetics and mechanism of the reaction between HCHO and benzene to form diphenylmethane (C<sub>13</sub>H<sub>12</sub>) on the MTH catalyst HZSM-5.

Martinez-Espin et al. proposed that diphenylmethane (DPM) is a product of HCHO condensation with benzene

(C<sub>6</sub>H<sub>6</sub>) during MTH catalysis on HZSM-5 at temperatures in the range of 523-623 K. During co-reaction of C<sub>6</sub>H<sub>6</sub> with CH<sub>3</sub>OH, a kinetic isotope effect for DPM formation was observed when using CD3OH as the reactant, suggesting that C-D bond cleavage was the rate-determining step for DPM formation. These claims were corroborated by the authors by noting that the molecular weight of the DPM product increased by two atomic mass units when using CD<sub>3</sub>OH as the reactant instead of CH3OH and by density functional theory (DFT) calculations, which showed that a viable DPM formation pathway involves HCHO alkylation of benzene to form a benzyl alcohol intermediate followed by condensation with benzene to form DPM and water. These observations led the authors to propose the reaction mechanism depicted in Scheme 1, where hydrogen abstraction from methanol to form formaldehyde is the rate-limiting step, followed by reaction

Received: July 8, 2020 Revised: August 16, 2020 Published: August 18, 2020



Scheme 1. Mechanism of DPM Formation Proposed by Martinez-Espin et al., Where the Rate-Limiting Step (RLS) Is CH<sub>3</sub>OH Dehydrogenation a

$$\begin{array}{c} H \\ H \\ O \\ OH \\ H \\ O \\ AI \\ CH_3OH \\ CH_3OH \\ CH_2O \\$$

"Climent et al." proposed a pathway from HCHO and C<sub>6</sub>H<sub>6</sub> involving a phenylmethelium ion intermediate (dashed lines).

with two benzene molecules and dehydration to form water and DPM. The work by Martinez-Espin et al. determined that the rate-determining step for DPM formation was methanol dehydrogenation. We investigate instead the kinetics and mechanism of DPM formation after the genesis of the HCHO species. Prior reports that investigate HCHO-mediated alkylation rates and pathways identify DPM as the highest selectivity product in the reaction between HCHO and C<sub>6</sub>H<sub>6</sub> on zeolite catalysts (HY and HZSM-5) during liquid-phase batch reactions.<sup>8,9</sup> Climent et al.<sup>9</sup> proposed a DPM formation mechanism on HY that is similar to the mechanism proposed by Martinez-Espin et al. for HZSM-5, with the exception that benzyl alcohol dehydrates to form a phenylmethelium ion (C<sub>7</sub>H<sub>7</sub><sup>+</sup>) before reaction with C<sub>6</sub>H<sub>6</sub> to form DPM<sup>+</sup> (dotted lines in Scheme 1). We report here the kinetics and mechanism of DPM at low partial pressures of HCHO (<0.5 kPa) and C<sub>6</sub>H<sub>6</sub> (<5 kPa) during gas-phase reaction.

Specifically, we investigate the kinetics and mechanism of DPM formation from HCHO and C<sub>6</sub>H<sub>6</sub> on self-pillared pentasil (SPP) HZSM-5 catalysts, a material with ~1.5 unit cell sheets of HZSM-5 chosen here to avoid complications due to diffusive transport. We observe transients during reaction, which were not reported in previous studies, and we demonstrate that these transients are the result of the slowly evolving fractional coverage of DPM<sup>+</sup> during reaction. Further, we show that DPM<sup>+</sup> is a persistent species that is formed and consumed by irreversible reactions in series, either of which can be rate-controlling depending on the reaction conditions. The deprotonation of DPM<sup>+</sup> is facilitated by aromatic species, such that the proton transfer from DPM<sup>+</sup> back to the zeolite is first-order in aromatics partial pressure. <sup>11</sup>

# 2. METHODS

**2.1. Catalyst Synthesis.** Self-pillared pentasil (SPP) HZSM-5 was chosen for this study because of its  $\sim$ 3 nm diffusion length scales to reduce potential complications arising from transport limitations. SPP-HZSM-5 was synthesized following a procedure reported previously,  $^{10,12}$  with a Si/Al ratio of 100 during synthesis. After synthesis, the zeolite was dried at 343 K for 12 h, followed by oxidative thermal treatment at 823 K for 12 h in air. The zeolite was then washed with distilled water and thrice ion-exchanged with a 1.0 mol  $L^{-1}$  ammonia nitrate solution at 353 K for 5 h, washed with water, dried at 343 K, and thermally treated in air at 823 K for 4 h to produce proton-form SPP-HZSM-5, assessed by amine

titration and temperature-programmed desorption (TPD, see Section 2.2).

2.2. Ammonia and 2,6-Di-tert-butylpyridine Temperature-Programmed Desorption (TPD). A gas stream containing 0.14 cm<sup>3</sup> s<sup>-1</sup> NH<sub>3</sub> (Praxair, 1% in He) diluted in 1.42 cm<sup>3</sup> s<sup>-1</sup> He and 0.167 cm<sup>3</sup> s<sup>-1</sup> Ar (internal standard) was fed to a fixed bed of 0.093 g of SPP-HZSM-5 heated to 423 K until 2 h after the NH3 concentration in the reactor effluent was the same as the reactor influent. Adsorbing NH<sub>3</sub> at 423 K titrates only the Brønsted-acidic sites in the framework and will not adsorb to Lewis-acidic aluminum in the zeolite channels. 13,14 An online mass spectrometer (MKS Instruments) was used to monitor the concentration of NH<sub>3</sub> (m/z =16) and Ar (m/z = 40) in the reactor effluent. The reactor bed was flushed at 423 K with 1.56 cm<sup>3</sup> s<sup>-1</sup> He and 0.167 cm<sup>3</sup> s<sup>-1</sup> Ar for at least 4 h to remove any physisorbed NH3 before heating at 0.167 K s<sup>-1</sup> to 723 K. The temperature was held at 723 K until the NH3 concentration in the effluent reached zero. The amount of NH3 that desorbed during the temperature ramp is considered to be stoichiometric with the number of Brønsted acid sites on the SPP-HZSM-5 catalyst. All gas flow rates in this study are at 298 K and atmospheric pressure.

A similar protocol was followed for the 2,6-di-tertbutylpyridine (DTBP) TPD experiments. A solution containing 0.048 g of DTBP (≥97%, Sigma-Aldrich) was added to 13.2 g of C<sub>6</sub>H<sub>6</sub>. The C<sub>6</sub>H<sub>6</sub>-DTBP solution was injected into a 1.12 cm<sup>3</sup> s<sup>-1</sup> He and 0.073 cm<sup>3</sup> s<sup>-1</sup> Ar (internal standard) stream via a syringe pump (KD Scientific) at a liquid flow rate of  $3.5 \times 10^{-4}$  cm<sup>3</sup> s<sup>-1</sup>. The stream was fed to a fixed bed reactor with 0.017 g SPP-HZSM-5 heated to 353 K for 1 h after the concentration of DTBP in the effluent was the same as the DTBP concentration in the influent. The reactor effluent was monitored by injection into a gas chromatograph (GC) equipped with a flame ionization detector (FID) and a thermal conductivity detector (TCD). After adsorption, the reactor bed was flushed at 353 K with He (1.12 cm<sup>3</sup> s<sup>-1</sup>) and Ar (0.073 cm<sup>3</sup> s<sup>-1</sup>) for 2 h. The reactor was then heated at 0.33 K s<sup>-1</sup> to 873 K in He  $(1.12 \text{ cm}^3 \text{ s}^{-1})$  and Ar  $(0.073 \text{ cm}^3 \text{ s}^{-1})$ , and the reactor effluent was monitored by GC-FID/TCD at 1 min intervals. The reactor temperature was held at 873 K until DTBP was no longer observed in the reactor effluent. The total moles of DTBP that desorbed during the temperature ramp was considered to be stoichiometric with the number of external Brønsted acid sites because the bulky tert-butyl groups

impede the diffusion of DTBP into the microporous channels of the SPP-HZSM-5 zeolite. <sup>10,15</sup>

2.3. Transient and Steady-State Diphenylmethane Rate Measurements. A solution of HCHO and H2O was prepared by adding H2O (Fisher Chemical, HPLC-grade submicron-filtered) to a HCHO/H2O solution (Thermo Scientific, 16% w/v HCHO in H<sub>2</sub>O, methanol-free) in ratios dependent on the reaction conditions. The HCHO/H2O solution, additional H2O feed, and C6H6 (Sigma-Aldrich, ACS reagent, ≥99.0%) were injected via syringe pumps (KD Scientific, Cole-Parmer) into a stream of 2.07 cm<sup>3</sup> s<sup>-1</sup> He and 0.073 cm<sup>3</sup> s<sup>-1</sup> Ar (internal standard) via heated liquid injection ports. The temperature of the injection ports varied with the liquid flow rate and reactant to achieve stable flows. A 1000 cm<sup>3</sup> mixing volume located downstream of the liquid injection ports was used to stabilize the concentrations of the reactor feed. The reactant stream was carried to and from one of two identical reactors via stainless steel lines heated to at least 353 K. The packed bed reactor is an annulus (0.4 cm od; 0.16 cm id) with a thermowell containing a K-type thermocouple that measures the temperature at the radial and axial centers of the packed bed. The outer wall of the annulus is borosilicate glass-lined stainless steel (SGE Analytical Science) and the inner wall is stainless steel. The reactor bed is heated externally by a resistive heating element (ARi Industries Inc.) controlled by a Watlow temperature controller. Reactant stream pressures are monitored by a pressure-transducer upstream of the reactor. Gas flows are controlled by mass-flow controllers (Brooks).

The SPP-HZSM-5 samples were crushed using a mortar and pestle and pressed to a pressure of 4000 psi, crushed again, and sieved between mesh 40 and 80 to obtain catalyst pellets of size 180–420  $\mu$ m. SPP-HZSM-5 catalyst particles (0.0109–0.0122 g) were physically mixed with quartz sand (~0.1 g, acid-washed with 2 M HNO<sub>3</sub>, rinsed with deionized water, and heated to 1273 K in flowing air for 12 h) and loaded into a reactor. Quartz wool was loaded before and after the reactor bed to keep it in place. Diphenylmethane formation rates were measured from 353 to 393 K at differential conversion ( $\leq$ 3.4% conversion HCHO,  $\leq$ 1%  $C_6H_6$ ) conditions. A discussion on heat and mass transport limitations can be found in Section S1 of the Supporting Information.

Diphenylmethane was the major product (typically >99 mol % selectivity, at minimum 82 mol % selectivity) under all reaction conditions studied. The reactor effluent was monitored by an online Agilent 7890 A gas chromatograph (GC) equipped with a flame ionization detector (FID) and a thermal conductivity detector (TCD). Hydrocarbon species (HCHO, C<sub>6</sub>H<sub>6</sub>, DPM, etc.) were separated on an Agilent HP-1 column (50 m  $\times$  0.320 mm) and quantified in the FID. Nonhydrocarbon species (H<sub>2</sub>O, Ar) were separated in an HP-Plot-Q (60 m × 0.320 mm) column and quantified in the TCD. The signal peaks in the FID and TCD chromatograms of the reactor effluent were assigned by comparison to chromatograms of known compounds injected into the GC, in addition to taking 10 cm<sup>3</sup> gaseous samples from the reactor effluent via a gas-tight syringe and injecting this sample into a gas chromatograph-mass spectrometer (GC-MS) to obtain the mass spectra of the various products.

The catalyst bed was regenerated between successive experiments by oxidative thermal treatments by flowing  $1.67 \, \text{cm}^3 \, \text{s}^{-1}$  zero-grade air through the catalyst bed beginning at the reaction temperature and heating at  $0.0167 \, \text{K s}^{-1}$  to  $823 \, \text{K}$ 

and holding for 6 h. The rate per mass of SPP-HZSM-5 degrades over repeated regenerations. This loss of activity is attributed to dealumination and collapse of the framework during thermal treatment, leading to the degradation of the catalyst and loss of active sites. To account for this loss of sites, a reference condition (0.010 kPa HCHO, 4 kPa H<sub>2</sub>O, 0.44 kPa C<sub>6</sub>H<sub>6</sub>, 393 K) was repeated regularly to determine the fractional activity remaining. The decrease in rate per mass catalyst was assumed to degrade linearly between reference tests. The change in rate per mass catalyst over time for each reactor bed is shown in Figure S3 of Section S2 in the Supporting Information. Typically, only one steady-state rate per reactor bed was measured per day. Sometimes, more than one steady-state rate was obtained per experiment by changing the reactant pressures after acquiring a previous steady-state data point. During these experiments, the first reaction condition was repeated at the end of the day to ensure the catalyst deactivated by less than 15% between the first and last steady-state rate measurements.

2.4. Steady-State Isotopic Transient Kinetic Analysis (SSITKA). SSITKA was used to determine the identity and fractional coverage of surface intermediates during steady-state reaction. During reaction,  $^{12}C_6H_6$  and  $^{13}C_6H_6$  ( $\geq 99\%$   $^{13}C_8$ , Sigma-Aldrich) were fed in parallel via syringe pumps into heated He carrier streams to opposite inlets of a Valco fourway valve (located downstream of mixing volumes varying in size from 100 to 1000 cm<sup>3</sup>) that selected which among the <sup>12</sup>C- or <sup>13</sup>C-labeled stream was fed to the reactor. After the four-way valve, the C<sub>6</sub>H<sub>6</sub> stream sent to the reactor was combined with the stream carrying HCHO, H<sub>2</sub>O, 2.07 cm<sup>3</sup> s<sup>-1</sup> He, and 0.073 cm<sup>3</sup> s<sup>-1</sup> Ar and this mixed gas stream was fed to the reactor. Initially,  $^{12}C_6H_6$  is fed to the reactor with HCHO and H<sub>2</sub>O until the DPM formation rate was invariant in time for ~45 min (three consecutive GC injections), i.e., steady state, as monitored by GC (Agilent 7890 A) equipped with an HP-1 column connected to an Agilent 5975c mass spectrometer (MS). After the reaction was at steady state, the four-way valve was flipped to feed \$^{13}C\_6H\_6\$ to the reactor and vent <sup>12</sup>C<sub>6</sub>H<sub>6</sub>. The isotopologue distribution and effluent composition were monitored by GC-MS until the product isotopologue distribution reached steady state. SSITKA was performed at two reaction conditions: 393 K, 0.02 kPa HCHO, 4 kPa H<sub>2</sub>O, 0.4 kPa C<sub>6</sub>H<sub>6</sub> and 393 K, 0.2 kPa HCHO, 2 kPa H<sub>2</sub>O, 0.4 kPa C<sub>6</sub>H<sub>6</sub>.

# 3. RESULTS AND DISCUSSION

**3.1. Amine Titration of Acid Sites.** The density of internal and external acid sites on the SPP-HZSM-5 catalyst was assessed by NH<sub>3</sub> and 2,6-di-*tert*-butylpyridine (DTBP) temperature-programmed desorption (TPD). Ammonia adsorbs onto both internal and external Brønsted acid sites, while the bulky *tert*-butyl groups on DTBP prevent the diffusion of DTBP into the micropores of the zeolite channels and thus only titrate the external Brønsted acid sites. <sup>10,15</sup> The amount of adsorbed titrant for each amine is reported in Table 1. The amine desorption profiles are shown in Figure S3 in Section S3

Table 1. Moles of Amine Titrant Adsorbed on SPP-HZSM-5

amine titrant	moles adsorbed ( $\mu$ mol g $^{-1}$ )
$NH_3$	141.2
DTBP	56.6

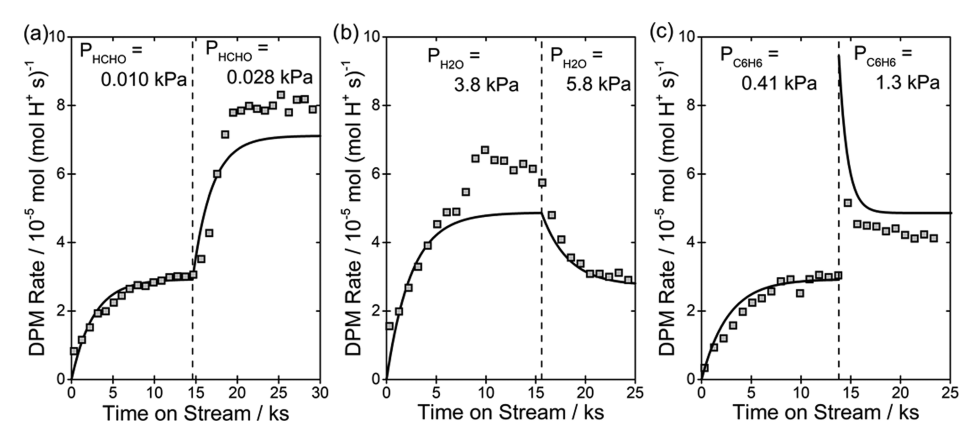


**Figure 1.** Transients observed starting from fresh catalyst (t = 0) and after step-changes in the partial pressure of a reactant (dashed line). The solid lines are the predicted rates based on a model with two irreversible reactions in series using parameters estimated from steady-state rate measurements. (a) Step-change in the HCHO pressure from 0.010 to 0.028 kPa with T = 393 K, 0.41 kPa  $C_6H_6$ , 3.7 kPa  $H_2O_5$  (b) step-change in the  $H_2O_5$  pressure from 3.8 to 5.8 kPa with T = 393 K, 0.41 kPa  $H_2O_5$  (b) step-change in the  $H_2O_5$  pressure from 3.8 to 5.8 kPa with  $H_2O_5$  pressure from 0.41 to 1.3 kPa with  $H_2O_5$  kPa HCHO, and 3.7 kPa  $H_2O_5$  kPa H2O.

of the Supporting Information. The small effective crystallite size of SPP-HZSM-5 results in a greater fraction of acid sites on the external surface of the catalyst compared to typical HZSM-5 catalysts. For the material used in this study, ~40% of acid sites are on the external surface, in line with previous reports. The DPM rate per acid site was slightly higher for internal + external acid sites than internal sites only, suggesting that external acid sites are more active than internal sites for DPM formation, as reported in Figure S4 in Section S4 of the Supporting Information. This effect may be a result of lower deprotonation energies or lower effective dielectric constants at the external surface compared to internal sites or other electrostatic interactions that arise as a result of confining voids. 16,17

3.2. Transient Step-Change Measurements. Transients in the rate of diphenylmethane formation lasting several hours are observed during the reaction between HCHO and C<sub>6</sub>H<sub>6</sub> on HZSM-5 when starting the reaction with a fresh catalyst or when a reaction condition is changed. The transients observed when starting from fresh catalyst (at time t = 0) and after stepchanging the pressure of HCHO, H<sub>2</sub>O, and C<sub>6</sub>H<sub>6</sub> are depicted in Figure 1. When the partial pressure of HCHO or H<sub>2</sub>O is step-changed (Figure 1a,b), the rate appears to change monotonically and continuously to a new steady-state value. In contrast, the rate appears to change discontinuously when the partial pressure of  $C_6H_6$  is step-changed (Figure 1c). In these experiments, the rate is not measured continuously and thus it is not possible to definitively determine whether the rate is continuous or discontinuous when each reactant pressure is step-changed; however, it is clear that there are two important time scales for the transient observed when step-changing C<sub>6</sub>H<sub>6</sub> partial pressure—the time scale for partial pressure changes (within one GC injection, <12 min) and the time scale for reaching steady state (1-3 h). Comparison of the transients strongly suggests that the rate is nearly discontinuous when changing the partial pressure of C<sub>6</sub>H<sub>6</sub>. The validity of this hypothesis is evaluated in Section 3.4.

Transients are ubiquitous in catalysis and provide essential information about the underlying reaction mechanism. These disparate time scales in the transients observed during stepchanges in partial pressures can be leveraged to elucidate the partial pressure dependencies of various steps in the DPM reaction mechanism as we discuss below. The observed rate of

DPM formation is a sum of the rates of all elementary step reactions multiplied by the stoichiometric coefficient of DPM (eq 1)

$$r_{\text{DPM}}(t)/L = \sum_{i} \nu_{i,\text{DPM}} r_i(t)$$

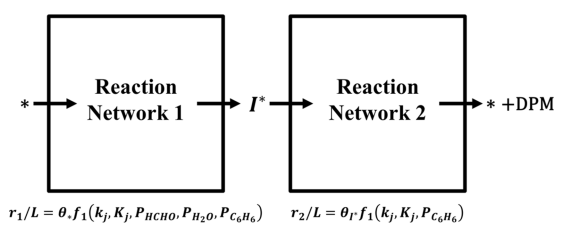
$$= \sum_{i} \nu_{i,\text{DPM}} k_i \prod_{j^*} (\theta_{j^*}(t))^{\alpha_{i,j^*}} \prod_{j} (P_j(t))^{\alpha_{i,j}}$$
(1)

where L is the number of active sites,  $\nu_{i,\text{DPM}}$  is the stoichiometric coefficient for DPM in reaction i,  $\theta_{i^*}$  is the fractional coverage of surface intermediate  $j^*$ ,  $P_i$  are the partial pressures for reactants j, and  $\alpha_{i,j}$  and  $\alpha_{i,j}$  are the reaction orders of surface intermediates  $j^*$  and reactants j for reaction i, respectively. In eq 1, it is assumed that the number of active sites, rate constants, stoichiometric coefficients, and reaction orders are invariant in time. The partial pressures only change at the start of the reaction and at the time of step-changes in partial pressures. In eq 1, the partial pressures change on time scales on the order of minutes, while the fractional coverages of surface species change in time with time scales that are dictated by the reaction kinetics and can be on the order of seconds to days. From eq 1, if there is a transient in the formation rate of a product over several hours, this necessarily requires that the fractional coverages of surface species are changing in time. It is assumed that the number of active sites is constant, but this quantity can change if (i) active sites are lost to deactivation or (ii) the structure of the catalyst is evolving. The transients observed in this system often involve rate increasing in time (Figure 1), which would require a concomitant increase in the number of active sites with time on stream. Unmodified, welldefined proton-form zeolite catalysts do not form additional sites with time on stream except during oxidative thermal treatment to remove deposited carbon, and thus, for this system, slowly evolving surface coverages with time on stream offer the most likely explanation for the transients observed.

The observed transients in rate are  $\sim 1-3$  h, suggesting that there is at least one kinetically relevant surface intermediate that requires several hours to reach a steady-state fractional coverage. This occurs when the rates of the reactions that form and consume the reaction intermediate are "slow" (relative to other important time scales in the reaction and to the data-

sampling rate). Knowing that the formation and consumption rates of at least one reaction intermediate are slow compared to those of other reactions in the overall reaction network, we propose a mechanistic description where the overall reaction network can be separated into two subreaction networks depicted in Scheme 2. In this mechanism, the network of

Scheme 2. Proposed Reaction Mechanism Based on Transients in DPM Rate with Step-Changes in Reactant Partial Pressures, as Shown in Figure  $1^a$ 



"Reactions in reaction network 1 and reaction network 2 are assumed to be at pseudo-steady-state conditions at much shorter time scales than the pseudo-steady-state assumption is valid for the reaction intermediate I\*.

reactions that form (reaction network 1) and consume (reaction network 2) the reaction intermediate,  $I^*$ , reaches a pseudo-steady state at much shorter time scales than the time scale required for the pseudo-steady-state assumption to be valid on the intermediate  $I^*$ . Hence, we can treat the rate functions of the subreaction networks as pseudo-steady-state rate functions ( $r_1$  for the formation of  $I^*$  and  $r_2$  for the consumption of  $I^*$ ), even during the transient when the pseudo-steady-state approximation on  $I^*$  is invalid, such that eq 2 describes the fractional coverage of  $I^*$  in time

$$\frac{\mathrm{d}\theta_{1^*}}{\mathrm{d}t} = \frac{r_1(t)}{L} - \frac{r_2(t)}{L} \tag{2}$$

The reaction rate for the consumption of I\* is then equal to the rate of DPM formation  $(r_2)$  and can be written as eq 3

$$r_2(t)/L = \theta_{1*}(t)f_2(k_j, K_j, P_{HCHO}(t), P_{C_6H_6}(t), P_{H_2O}(t))$$
(3)

where  $r_2$  is the rate of DPM formation, L is the number of active sites,  $k_j$  and  $K_j$  are the elementary step rate and equilibrium constants, respectively,  $\theta_{1^*}$  is the fractional surface coverage of the reaction intermediate,  $I^*$ , and  $f_2$  is a function that describes the dependencies of the elementary step rate on  $k_j$ ,  $K_j$ , and the reactant partial pressures,  $P_i$ . Equation 3 is written with only one surface species in the elementary step because zeolites do not typically catalyze reactions involving two sites, especially in high Si/Al materials like the catalyst used in this study. From eq 3, the pressure dependencies of the rate function for the consumption of  $I^*$  can be probed by studying the transient rate during step-changes in the partial pressure of each reactant, as is demonstrated herein.

The continuity or discontinuity in the transient rate when step-changing the partial pressure of each reactant provides insights about the pressure dependencies of the steps comprising the composite reaction network. During the transient rate measurements shown in Figure 1, the reactant partial pressures only change at the start of the experiment (t = 0) and at the time of the step-change (indicated by dashed lines) and reach stable values within minutes. At the time of

the step-change, the partial pressure of a species changes nearly discontinuously (e.g., benzene pressure changes from 0.41 to 1.3 kPa at the dashed line for the data shown in Figure 1c). If the function  $f_2$  in eq 3 depends on these partial pressures, its value will also change discontinuously, which in turn will result in a discontinuity in the rate of DPM formation,  $r_2$ , because the rate is changing on the time scale that the partial pressures are changing. In this way, by monitoring whether the reaction rate undergoes a near-discontinuous change when reactant partial pressures are step-changed, the functional dependence of  $f_2$  can be ascertained. From Figure 1, the rate changes discontinuously only when the partial pressure of  $C_6H_6$  is step-changed, and thus we conclude (eq 4)

$$f_2 = f_2(k_i, K_j, P_{C_6H_6}(t)) \tag{4}$$

such that the formation of the final DPM product, which is the net rate of reaction network 2 in Scheme 2, is a function only of the fractional coverage of  $I^*$  and the partial pressure of  $C_6H_6$  and does not depend on the partial pressures of  $H_2O$  or HCHO.

The steady-state DPM rate changes as a function of HCHO and  $H_2O$  partial pressures, as shown in Figure 1a,b. Because the rate  $r_2$  does not depend on HCHO and  $H_2O$  partial pressures, the rate function for the formation of  $I^*$ ,  $r_1$ , must depend on the partial pressures of these reactants. During a step-change in the  $C_6H_6$  partial pressure, a discontinuity is observed if the rate function  $r_2$  is a function of the benzene partial pressure, regardless of whether the rate function  $r_1$  is a function of the  $C_6H_6$  partial pressure. Thus, from the transient data shown in Figure 1, it is not possible to determine with certainty whether the rate of formation of the surface intermediate,  $I^*$ , depends on the partial pressure of  $C_6H_6$ ; therefore, the formation rate of the surface intermediate  $(r_1)$  is assumed to be of the form given in eq 5 to include the possibility of rates depending on the  $C_6H_6$  partial pressure

$$r_1/L = \theta_*(t) f_1(k_i, K_i, P_{HCHO}(t), P_{H,O}(t), P_{C_kH_k}(t))$$
 (5)

The dependency of this rate on the partial pressure of  $C_6H_6$  is assessed by steady-state rate measurements by varying the  $C_6H_6$  pressure at conditions where the formation of I\* is known to be rate-controlling for DPM formation (see Section 3.3).

We recently extended the concept of rate-controlling steps to non(pseudo)steady-state rates; the method developed therein enables analytical relationships between features of the transient rate (e.g., discontinuities and extrema) during step-changes in the reactant pressure and the pressure dependencies of the elementary step reactions. At the time of a step-change, only steps that consume or form the final product are rate-controlling because the fractional coverages depend solely on the initial condition at this time and are not functions of the rate constants, such that the DPM rate is given by a function of the form (eq 6)

$$\frac{r_2(t=t_{0^+})}{L} = f_2(k_j, K_j, P_{C_6H_6})\theta_{1^*,0}$$
(6)

where  $t_0$  is the time immediately after the step-change and  $\theta_{1*,0}$  is the fractional coverage of I\* at the time of the step-change. For the transients observed in Figure 1, we see that the rate at the time of the step-change depends on the partial pressure of  $C_6H_6$  but not on the partial pressures of HCHO or  $H_2O$  because a discontinuous change in the rate is observed only

when step-changing the partial pressure of C<sub>6</sub>H<sub>6</sub>. Further, the step that is rate-controlling at the time of the step-change is likely not rate-controlling at steady state at these reaction conditions since the steady-state rate is a function of HCHO and H<sub>2</sub>O pressures (Figure 1). Thus, at the reaction conditions in Figure 1, we conclude that the rate-controlling step is changing as a function of time, where (i) at the start of the transient, the consumption of I\* to form DPM is ratecontrolling and is a function only of the C<sub>6</sub>H<sub>6</sub> partial pressure and (ii) at steady state, the formation of I\* is rate-controlling and is a function of HCHO and H2O partial pressures. Thus, the partial pressure dependencies of the initial (at time  $t = t_0$ ) immediately after the step-change) and steady-state rates and the observed transients during step-changes in the partial pressure are rationalized by degrees of rate control at non(pseudo)steady-state conditions. Discussion on how the degrees of rate control for DPM formation evolve during each of the transients in Figure 1 can be found in Section S5 of the Supporting Information.

From transient step-change experiments, we identified that there are two rate functions that describe the rate of DPM formation—one function for the formation of a surface intermediate, I\*, and another function for the consumption of the surface intermediate to form the final product, DPM. The surface intermediate, I\*, does not rapidly reach a steady-state fractional coverage, but instead changes slowly in time with each change in the reaction condition, resulting in a transient in the DPM formation rate. In the next section, we report and discuss observations from measured steady-state reaction rates to obtain a detailed mechanistic description for reaction networks 1 and 2 in Scheme 2 and identify potential rate-controlling transition states for DPM formation.

**3.3. Steady-State Rate Measurements.** The reaction temperature and partial pressures of HCHO,  $\rm H_2O$ , and  $\rm C_6H_6$  were systematically varied to investigate the steady-state kinetics of DPM formation. The rate measurements were obtained under differential conversion conditions ( $\leq$ 3.4% HCHO,  $\leq$ 1%  $\rm C_6H_6$ ). In total, 153 independent steady-state rate measurements were obtained. These data are tabulated in Table S1 in Section S6 of the Supporting Information, and a subset of these data are reported in Figures 2 and 3.

In Figure 2a, at low HCHO pressures, the DPM formation rate is first-order in HCHO. From the transient step-change experiments, we determined that the rate of formation of the surface intermediate, I\*, was a function of the partial pressure of HCHO, but the rate of consumption of this intermediate depends only on the C<sub>6</sub>H<sub>6</sub> partial pressure. The rate of I\* formation is likely at most first-order in HCHO because only one HCHO molecule appears in the overall reaction, and because the overall rate at low HCHO pressure is first-order in HCHO, the formation of the surface intermediate is likely the rate-controlling step at this condition. The unfilled data points indicated by the star in Figure 2a,c are at the same reaction condition, where the reaction is first-order in HCHO and also nonzero-order in benzene. Thus, the rate of I\* formation is a function of benzene pressure and the functional dependence of  $f_1$  includes dependence on benzene partial pressure, as reported above in eq 5.

Inhibition by  $H_2O$  is more significant at low benzene pressures (Figure 3), where the reaction is first-order in benzene (Figure 2c), than at high benzene pressures, where the reaction order of benzene is zero. This simultaneous change in reaction orders suggests that both  $H_2O$  and  $C_6H_6$  compete for

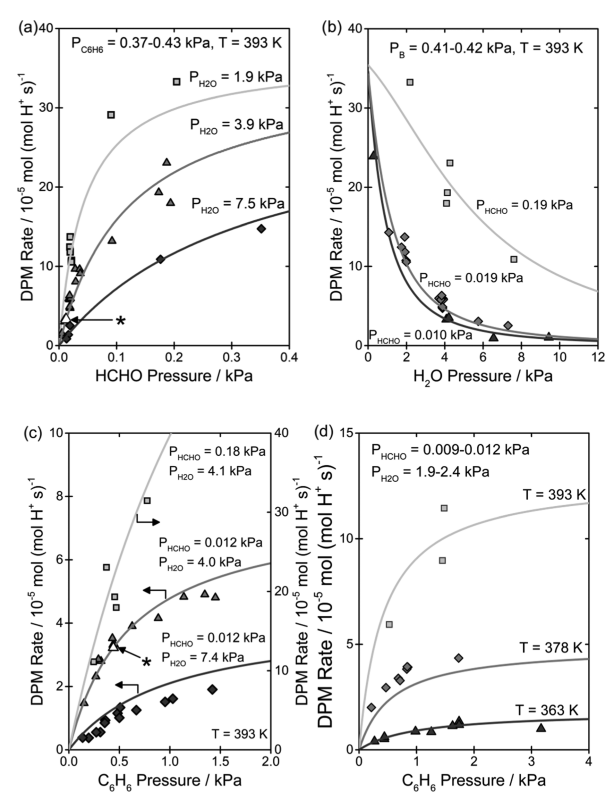


**Figure 2.** Steady-state rates at varying reaction conditions. (a) Rate as a function of the HCHO pressure with  $T=393~\rm K$ ,  $0.37-0.43~\rm kPa$   $C_6H_6$ , with varying  $H_2O$  pressures (1.9, 3.9, and 7.5 kPa). (b) Rate as a function of the  $H_2O$  pressure with  $T=393~\rm K$ ,  $0.41-0.42~\rm kPa$   $C_6H_6$ , and varying HCHO pressures (0.010, 0.019, and 0.19 kPa). (c) Rate as a function of the  $C_6H_6$  pressure at  $T=393~\rm K$ , at varying conditions: squares, 0.18 kPa HCHO, 4.1 kPa  $H_2O$ ; diamonds, 0.012 kPa HCHO, 4.0 kPa  $H_2O$ ; and triangles, 0.012 kPa HCHO, 7.4 kPa  $H_2O$ . (d) Rate as a function of the  $C_6H_6$  pressure at varying temperatures (T=363, 378, and 393 K) with 0.009-0.012 kPa HCHO, 1.9-2.4 kPa  $H_2O$ . The lines are the model fits to the experimental data (see Section 3.5). Stars (\*) pointing to the unfilled symbols in (a) and (c) indicate the same experimental conditions.

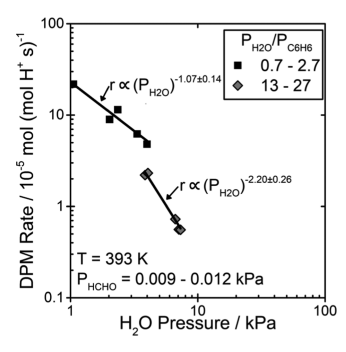


**Figure 3.** Plot of rate versus  $\rm H_2O$  pressure at (square) low and (diamond) high  $P_{\rm H_2O}/P_{\rm C_6H_6}$  ratios at 393 K, 0.009–0.012 kPa HCHO and (square) 1.39–1.48 kPa  $\rm C_6H_6$ , (diamond) 0.27–0.31 kPa  $\rm C_6H_6$ . The lines are the power-law fits, where the power is the apparent reaction order of  $P_{\rm H_2O}$ .

the same site and, depending on their respective pressures, either  $\rm H_2O^*$  or  $\rm C_6H_6^*$  surface species dominate. A plausible mechanism that agrees with these steady-state and transient rate data is shown in Scheme 3, where the adsorbed HCHO, which is in competition with the adsorption of  $\rm C_6H_6$  and  $\rm H_2O$ ,

# Scheme 3. Proposed Reaction Network for the Formation of DPM

$$K_{C6H6} + C_6H_6$$
 $K_{C6H6} + C_6H_6$ 
 $K_{HCHO} + K_{HCHO} + K_$ 

reacts with benzene to form the surface intermediate, I\*, which further reacts with  $C_6H_6$  (see eq 4) to form DPM. In addition to being inhibited by the adsorption of  $H_2O$  on acid sites, the reaction is also inhibited by HCHO hydration by  $H_2O$  to form methane diol ( $CH_4O_2$ ), as reported by Bollini et al., <sup>19</sup> giving a minimum reaction order of -2 in water.

Methane diol was not observed; however, the decomposition of  $CH_4O_2$  to  $H_2O$  and HCHO occurs in the gas phase  $^{20-23}$  and may occur in the stainless steel lines (heated up to 473 K) or in the GC inlet (heated to 473 K), both maintained at elevated temperatures where HCHO becomes more thermodynamically favorable than methane diol. <sup>19</sup> An alternative explanation for the observed reaction orders in  $H_2O$  and  $C_6H_6$  is the formation of  $H_2O-H_2O$  and  $C_6H_6-H_2O$  dimers instead of the formation of methane diol (Scheme 3), but these mechanistic hypotheses are kinetically indistinguishable. In Scheme 3, the equilibrium between HCHO and  $CH_4O_2$  is described by eq 7

$$K_{\text{hyd}} = \frac{P_{\text{CH}_4\text{O}_2}}{P_{\text{H}_2\text{O}}P_{\text{HCHO}}} \tag{7}$$

where  $K_{\rm hyd}$  is the pressure equilibrium constant for HCHO hydration and  $P_j$  are the equilibrium partial pressures of CH<sub>4</sub>O<sub>2</sub>, H<sub>2</sub>O, and HCHO. By mole balance under differential conversion conditions, the partial pressures of HCHO and CH<sub>4</sub>O<sub>2</sub> sum to the partial pressure of the inlet HCHO,  $P_{\rm HCHO,0}$  (eq 8)

$$P_{\text{HCHO}} + P_{\text{CH}_4O_2} = P_{\text{HCHO},0} \tag{8}$$

Combining eqs 7 and 8, the partial pressure of HCHO during reaction,  $P_{\rm HCHO}$ , is related to the HCHO pressure fed to the reactor,  $P_{\rm HCHO,0}$ , by eq 9

$$P_{\text{HCHO}} = \frac{P_{\text{HCHO,0}}}{1 + K_{\text{hyd}} P_{\text{H}_2\text{O}}} \tag{9}$$

where HCHO pressures reported in this work are  $P_{\rm HCHO,0}$ . The rate function for the formation of I\* from the reaction network shown in Scheme 3 (see Section S7 in the Supporting Information for derivation) is thus given by eq 10

$$r_{1}/L = \frac{k_{1}K_{\text{HCHO}}P_{\text{HCHO},0}P_{\text{C}_{6}\text{H}_{6}}/(1 + K_{\text{hyd}}P_{\text{H}_{2}\text{O}})}{1 + \frac{K_{\text{HCHO}}P_{\text{HCHO},0}}{1 + K_{\text{hyd}}P_{\text{H}_{2}\text{O}}} + K_{\text{C}_{6}\text{H}_{6}}P_{\text{C}_{6}\text{H}_{6}} + K_{\text{H}_{2}\text{O}}P_{\text{H}_{2}\text{O}}}\theta_{*'}}$$
(10)

where  $\theta_{*'} = \theta_* + \theta_{\text{HCHO}^*} + \theta_{\text{C}_6\text{H}_6^*} + \theta_{\text{H}_2\text{O}^*} = 1 - \theta_{\text{I}^*}$  is the fractional coverage of all species that are equilibrated with vacant proton sites. The rate of I\* consumption to form DPM in Scheme 3 is an elementary step with the rate given by eq 11

$$r_2/L = k_2 P_{C_6 H_6} \theta_{I^*} \tag{11}$$

Combining eqs 10 and 11 and noting that at steady state  $r_1 = r_2$  and at all times  $\theta_{*'} = 1 - \theta_{1*}$ , the rate function for DPM formation for the composite reaction shown in Scheme 3 is (eq 12)

$$r_{\text{DPM}}/L = \frac{k_1 k_2 K_{\text{HCHO}} P_{\text{HCHO},0} P_{\text{C}_6 \text{H}_6} / (1 + K_{\text{hyd}} P_{\text{H}_2 \text{O}})}{\frac{k_1 K_{\text{HCHO}} P_{\text{HCHO},0}}{1 *} + \underbrace{k_2}_{*} + \underbrace{\frac{k_2 K_{\text{HCHO}} P_{\text{HCHO},0}}{1 + K_{\text{hyd}} P_{\text{H}_2 \text{O}}}}_{\text{HCHO*}} + \underbrace{k_2 K_{\text{C}_6 \text{H}_6} P_{\text{C}_6 \text{H}_6}}_{\text{C}_6 \text{H}_6} + \underbrace{k_2 K_{\text{H}_2 \text{O}} P_{\text{H}_2 \text{O}}}_{\text{H}_2 \text{O}}}_{\text{H}_2 \text{O}}}$$
(12)

where each term in the denominator corresponds to the fractional coverage of a surface species, indicated by the brackets. Equation 12 shows the full rate function for the reaction in Scheme 3. Many terms in the denominator of eq 12 are negligible because the corresponding species have low fractional coverages, and thus multiple kinetic/thermodynamic

parameters are not estimable from the kinetic data, which requires us to simplify eq 12 to only include relevant quantities.

At high HCHO pressures, the rate becomes zero-order in HCHO (Figure 2a). This can occur because (i) the HCHO coverage approaches unity and the formation of  $I^*$  is rate-controlling or (ii) the coverage of  $I^*$  approaches unity and the consumption of  $I^*$  becomes rate-controlling at high HCHO

pressures, whose rate function depends on only the benzene partial pressure (eq 11). If (i) is true, then the third term in the denominator of eq 12 becomes much larger than all other denominator terms, and eq 12 simplifies to  $r_{\rm DPM}/L = k_1 P_{\rm C_6 H_6/P}$  which is order zero in water, order zero in HCHO, and order one in benzene. If (ii) is true, then the first term in the denominator of eq 12 becomes much larger than all other denominator terms, and eq 12 simplifies to  $r_{\rm DPM}/L = k_2 P_{\rm C_6 H_6/P}$  which is order zero in H<sub>2</sub>O, order zero in HCHO, and order one in benzene. These cases are indistinguishable from steady-state rate measurements.

From steady-state rate measurements, we identified that the formation of a reaction intermediate, I\*, is rate-controlling at least at low HCHO pressures and that the rate function for the formation of I\* depends on HCHO,  $H_2O$ , and  $C_6H_6$  partial pressures. A plausible reaction network for the formation and consumption of I\* was proposed (Scheme 3). Steady-state rate measurements were not able to ascertain whether the formation or consumption of I\* is rate-controlling at high HCHO pressures, where the reaction order of HCHO approaches zero. In the following section, we use isotopic switching experiments to assess the steady-state fractional coverage and identity of I\* to determine the rate-controlling steps of DPM formation.

**3.4. Steady-State Isotopic Transient Kinetic Analysis (SSITKA).** During SSITKA, the reactant feed was switched from  $^{12}C_6H_6$  to  $^{13}C_6H_6$  at steady state. After the isotopic switch, the surface intermediate formed prior to the switch will have  $^{12}C$ -labeled six-membered rings. The isotopic content of the first DPM product formed immediately after the isotopic switch depends on the number of six-membered rings in the surface intermediate, I\*, and the number of six-membered rings added to I\* from the gas phase to form DPM. The number of  $^{12}C$ -labeled aromatic rings in the first DPM product after the isotopic switch is equal to the number of six-membered rings in I\*.

The results of the isotopic switching experiments at two different reaction conditions are shown in Figure 4. At both reaction conditions, the first DPM product formed immediately after the switch has an m/z = 168, corresponding to entirely <sup>12</sup>C-labeled DPM. Only trace amounts of DPM

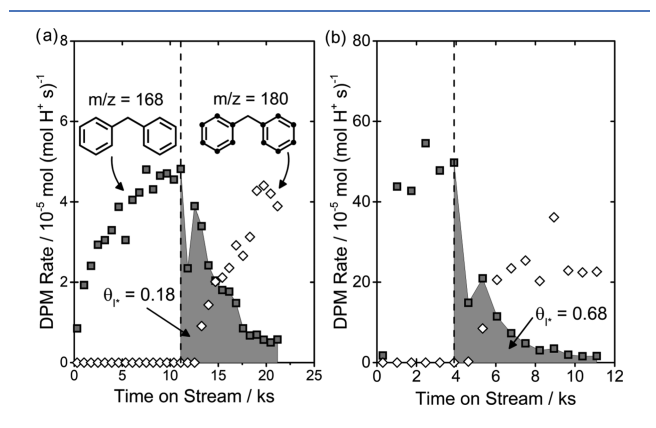


**Figure 4.** SSITKA experiments where  $^{12}C_6H_6$  is switched to  $^{13}C_6H_6$  at the dashed line. The shaded area under the curve is proportional to the fractional coverage of I\* at steady state. (a) 393 K, 0.02 kPa HCHO, 4 kPa  $H_2O$ , 0.4 kPa  $C_6H_6$ . The net rate of DPM is order  $\sim$ 1 in HCHO. (b) 393 K, 0.2 kPa HCHO, 2 kPa  $H_2O$ , 0.4 kPa  $C_6H_6$ . The net rate of DPM is order <1 in HCHO.

product with one labeled aromatic ring (m/z = 174) were observed. These data suggest that the reaction intermediate, I\*, has two six-membered rings. This is consistent with a protonated diphenylmethane benzenium ion ( $C_{13}H_{13}^+$ ) as I\*. Stable methylated DPM benzenium ions are important intermediates in alkylaromatic transalkylation pathways in zeolite catalysts, <sup>24–31</sup> including HZSM-5. <sup>26,27</sup> Computational calculations suggest deprotonation activation energies of methylated DPM<sup>+</sup> in TON<sup>30</sup> and FAU<sup>29</sup> zeolite catalysts of 70 and 75 kJ mol<sup>-1</sup>, respectively.

As the reaction progresses, all 12C-labeled I\* is consumed and replaced with 13C-labeled I\*, and an increase in DPM product with two  $^{13}$ C-labeled aromatic rings (m/z = 180) is observed. The total amount of the <sup>12</sup>C-labeled DPM product formed after the isotopic switch corresponds to the steadystate fractional coverage of I\*. Figure 4a shows the SSITKA results for a steady-state reaction condition where the rate of DPM formation is order ~1 in HCHO (low HCHO pressure), and Figure 4b shows the SSITKA results where the steadystate rate is order <1 in HCHO (high HCHO pressure). The corresponding steady-state fractional coverages of I\* (DPM+) for reaction order  $\sim 1$  and < 1 are 0.18 and 0.68, respectively. This suggests that the reaction order of HCHO changes not because the fractional coverage of HCHO\* is approaching unity but because the fractional coverage of DPM+ is approaching unity. For the irreversible formation  $(r_1)$  and consumption  $(r_2)$  of DPM<sup>+</sup>, the steady-state fractional coverage of DPM+ is related to the kinetic degrees of rate control by  $(eq 13)^{32}$ 

$$\theta_{\text{DPM}^{+}} = \frac{\sum_{i} s_{i} \nu_{i \text{DPM}^{+}} [\nu_{i \text{DPM}^{+}} < 0]}{\sum_{i} \sum_{n*} s_{i} \nu_{i n*} [\nu_{i n*} < 0]} = \frac{s_{2}}{s_{1} + s_{2}} = s_{2} = X_{\text{RC}, 2}$$
(13)

where eq 13 was simplified because  $\sum_i s_i = s_1 + s_2 = 1$  and related to  $X_{RC,2}$  by noting  $X_{RC,2} = s_2(1-Z_2) = s_2$  since the consumption of DPM<sup>+</sup> is assumed irreversible  $(Z_2=0)$ . Equation 13 shows that the measured fractional coverage of DPM<sup>+</sup> is equal to the kinetic degree of rate control of reaction 2, the consumption of DPM<sup>+</sup>. Thus, we conclude that the reaction order in HCHO is changing because the rate-controlling step is changing from the formation of DPM<sup>+</sup> at low HCHO pressures to the consumption of DPM<sup>+</sup> at high HCHO pressures.

The SSITKA results suggest that the reaction intermediate is DPM<sup>+</sup> and that, at high HCHO pressures, the consumption of the reaction intermediate to form the final product, DPM, is the rate-controlling step. However, transient rate measurements (Figure 1c) suggest that the rate of consumption of the reaction intermediate is a function of the benzene partial pressure. This is corroborated by steady-state rate measurements that show that at high HCHO pressures, the reaction order is ~1 in benzene (Figure 2c). These data suggest that the rate of proton transfer from DPM<sup>+</sup> back to the zeolite framework is facilitated by benzene.

To determine whether deprotonation of DPM<sup>+</sup> is assisted by the presence of aromatics, HCHO and benzene were reacted on HZSM-5 at 353 K until reaching steady-state reaction conditions to form DPM<sup>+</sup> inside the zeolite catalyst (phase I in Figure 5a). The reactor was then flushed with 2.07 cm<sup>3</sup> s<sup>-1</sup> He for 6 h at 353 K to remove any residual reactants and products. At the end of the He flush, no DPM was observed in the reactor effluent. After the He flush, a stream containing 0.4 kPa

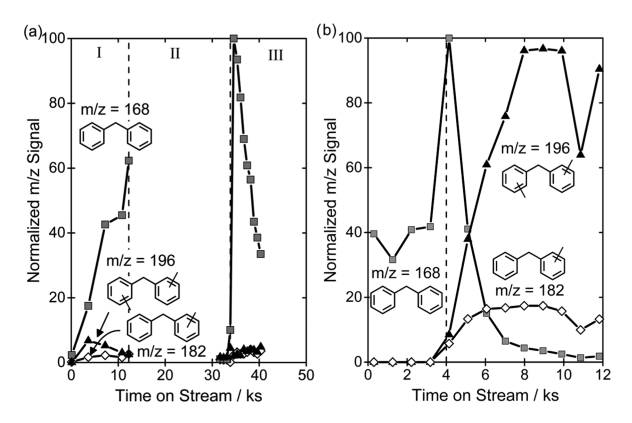


Figure 5. GC-MS data for DPM (m/z=168), methyl-DPM (m/z=182), and dimethyl-DPM (m/z=196) normalized within each figure. (a) During phase I (0–12 ks time on stream), 0.4 kPa  $C_6H_6$ , 0.2 kPa HCHO, and 2.0 kPa  $H_2O$  are fed to the reactor heated to 353 K to build up a surface coverage of DPM<sup>+</sup> species. During phase II (12–32 ks time on stream), the reactor was flushed with helium at 353 K. No DPM was observed at the end of the helium flush. During Phase III, 0.4 kPa toluene in helium was introduced to the reactor at 353 K. (b) At time on stream = 0 ks, the reaction is at steady state with T=393 K, 0.4 kPa  $C_6H_6$ , 0.012 kPa HCHO, and 4.0 kPa  $H_2O$ . At  $\sim$ 3 ks (dashed line), the feed was switched to a stream containing 0.4 kPa total aromatics with 2 toluene:1 benzene.

toluene was fed to the reactor. Immediately after introducing toluene to the reactor, unmethylated DPM was observed in the reactor effluent, demonstrating that DPM+ deprotonation is positive order in aromatics. The deprotonation of DPM<sup>+</sup> forms DPM, and thus, the rate is indeed discontinuous through the step-change in the partial pressure of  $C_6H_6$  (Figure 1c). The rate of DPM decreased with time on stream after introducing toluene as the fractional coverage of DPM<sup>+</sup> decayed to zero. In repeat experiments, toluene was replaced with cyclohexane after the He flush, but no DPM products were observed, suggesting that aromatics are necessary to facilitate the proton transfer from DPM<sup>+</sup> to the zeolite framework. Lower protontransfer energy barriers between aromatic molecules compared to nonaromatic molecules have been reported previously.<sup>34</sup> If this is the prevalent mechanism for aromatic-assisted proton transfer from DPM+ to the zeolite, once the proton is transferred from DPM+ to C<sub>6</sub>H<sub>6</sub>, the proton transfer to the zeolite framework must be spontaneous, as these benzenium ions are unstable in HZSM-5. 35,36 We hypothesize that a C<sub>6</sub>H<sub>7</sub><sup>+</sup> carbenium ion is not formed but instead forms a transition state comparable to that of H/D exchange of C<sub>6</sub>H<sub>6</sub> on zeolites, where the proton transfer to benzene from DPM<sup>+</sup> and from benzene to the zeolite is concerted.<sup>37</sup> During reaction, C<sub>6</sub>H<sub>6</sub> may act as a proton shuttle between DPM<sup>+</sup> and the zeolite framework as an organic cocatalyst for the deprotonation of DPM<sup>+</sup> in HZSM-5. Alternatively, the  $\pi$ system of aromatics may interact with the positively charged aromatic system in DPM+ species, lowering the energy barrier for deportation. The DPM+ surface species is persistent through a 6 h He flush, suggesting that its formation is irreversible, in agreement with the mechanism proposed in Scheme 3. This is in contrast to what Clark et al.<sup>31</sup> proposed for DPM-mediated transalkylation mechanisms of m-xylene on FAU catalysts, where they suggested based on DFT calculations that the formation of a DPM<sup>+</sup> species is reversible and will likely re-form the adsorbed alkylaromatic alkoxy species and gas-phase m-xylene many times before transferring the proton from DPM<sup>+</sup> to the zeolite. If this occurred during the present study, some DPM product with one <sup>13</sup>C-labeled aromatic ring would have been observed after the isotopic switch in the SSITKA experiment (Figure 4), and in Figure 5a, a significant amount of methyl-DPM would be expected when feeding toluene after the 6 h helium flush. Thus, we conclude that at the reaction conditions in this study, DPM<sup>+</sup> formation is not reversible.

Svelle et al.<sup>27</sup> observed DPMs (methyl- and dimethyl-DPM) upon dissolution of HZSM-5 after the reaction of toluene at 423 K for 16 h, demonstrating the importance of methylated DPM<sup>+</sup> intermediates in toluene disproportionation reactions. They examined the stability of the methylated DPM<sup>+</sup> intermediates by flushing several batches of prereacted catalysts at 473 K in N2 for 5 min to 2 h and dissolved each batch to liberate the entrained species. They observed a monotonic decrease in entrained DPMs and an initial increase in entrained xylenes with increasing flushing time, suggesting that dimethyl-DPM<sup>+</sup> decomposed to toluene and formed an adsorbed xylene alkoxy species. They did not report whether dimethyl-DPM was observed in the reactor effluent during the N<sub>2</sub> flush, so the rate of DPM<sup>+</sup> deprotonation relative to the rate of decomposition at these conditions is unknown. Regardless, methylated DPM<sup>+</sup> likely decomposes to single-ringed alkoxy aromatic species at temperatures elevated relative to those in the present study.

To ensure that no significant transport limitations impact the results of these transient experiments, we measured the rate of DPM products during a steady-state switch from a feed containing 0.4 kPa benzene to a feed containing 0.4 kPa aromatics with 2 toluene/1 benzene, while keeping the HCHO and H2O pressures constant. After the feed was switched, the rate of DPM formation increased in the injection immediately after the switch ( $\sim$ 12 min after switch), demonstrating that (i) toluene is more reactive than benzene for catalyzing the proton transfer from DPM<sup>+</sup> to the framework and (ii) the rate senses the change in feed composition on much shorter time scales (<12 min) than the time scale for transients in the observed rates ( $\sim$ 1-3 h), suggesting that the reactant concentration in the catalyst particle matches that of the reactant feed at short times on stream. Thus, we conclude that the transient kinetic measurements are not transport-limited (see Section S8 of the Supporting Information for a detailed explanation on transport effects during transients). After the reaction reaches steady state with the toluene-benzene feed, methylated DPM products are observed. This confirms that during the reaction between toluene and DPM+ after a He flush (Figure 5a), toluene is not incorporated into the final product, but instead only facilitates proton transfer from DPM+.

Through steady-state isotopic switching experiments, we determined that the reaction intermediate has two sixmembered rings and is likely a diphenylmethane benzenium ion. The fractional coverage of this benzenium ion during steady-state catalysis varies with the reaction condition and the HCHO reaction order varies with the fractional coverage of DPM<sup>+</sup>. At sparse DPM<sup>+</sup> coverages, the rate-controlling step is the formation of DPM<sup>+</sup> and the reaction is first-order in HCHO. At high coverages of DPM<sup>+</sup>, the rate-controlling step becomes the deprotonation of DPM<sup>+</sup> to form DPM, and the net rate of DPM formation approaches zero-order in HCHO. Combining all of this information, we propose a reaction mechanism and kinetic model for DPM formation that quantitatively describes the transient and steady-state reaction

Scheme 4. Reaction Mechanism for Diphenylmethane Formation

rates with reactant partial pressures ranging from 0.005 to 0.35 kPa HCHO, 0.14 to 4.1 kPa  $C_6H_6$ , and 0.11 to 12.5 kPa  $H_2O$  and the temperature varying from 363 to 393 K.

3.5. Reaction Mechanism and Kinetic Model. The DPM formation mechanism presented in Scheme 4 arises from the combination of transient, steady state, and isotopic data to complete the mechanistic description shown in Scheme 3. In Scheme 4, the adsorbed HCHO reacts with benzene to form benzyl alcohol, as was proposed by Martinez-Espin et al.7 and Climent et al.9 However, benzyl alcohol was not observed in either of these studies. During reaction between 0.036 kPa benzyl alcohol (C<sub>7</sub>H<sub>7</sub>OH) and 7.2 kPa C<sub>6</sub>H<sub>6</sub> on SPP-HZSM-5 at 353 K, we did not observe any DPM product, despite nonzero rates of DPM formation during reaction between HCHO and C<sub>6</sub>H<sub>6</sub> at 353 K (see Figure S4 in the Supporting Information). This suggests that there may be an alternative route to DPM formation that bypasses a benzyl alcohol intermediate or that cofeeding of benzyl alcohol at pressures much higher than those present during the HCHO reaction with C<sub>6</sub>H<sub>6</sub> may significantly alter the reaction pathways such that no DPM product is formed. At reaction temperatures of 373 K and 393 K, DPM product was observed with 0.025 kPa  $C_7H_7OH$  and 4.0 kPa  $C_6H_6$  at similar residence times as HCHO reactions with C<sub>6</sub>H<sub>6</sub>. At all temperatures, complete conversion of benzyl alcohol is observed. When feeding only benzyl alcohol, the only products observed are benzaldehyde and toluene, which are known products of benzyl alcohol disproportionation on zeolite catalysts.<sup>38</sup> At very few reaction conditions during the HCHO reaction with C<sub>6</sub>H<sub>6</sub>, specifically when the coverage of DPM+ is high (i.e., high HCHO pressures), a quantifiable amount of benzaldehyde (<20 mol % of carbon-containing products) is observed, suggesting that benzyl alcohol, which is not observed at any reaction conditions, is formed during these reactions (see Section S9 of the Supporting Information for benzaldehyde rates as a function of the HCHO pressure). Benzyl alcohol is present in low enough pressures that it is not observed during reaction, suggesting that it is a reactive intermediate that is rapidly consumed by forward or reverse reaction. Decomposition of benzyl alcohol to benzene and HCHO was not observed when reacting only benzyl alcohol on SPP-HZSM-5, suggesting that benzyl alcohol must be consumed rapidly by forward reactions to form DPM<sup>+</sup> or benzaldehyde byproducts. From these data, we conclude that the rate-controlling step of DPM<sup>+</sup> formation is the C-C bond formation between HCHO and C<sub>6</sub>H<sub>6</sub>, in agreement with the steady-state kinetics being at most firstorder in C<sub>6</sub>H<sub>6</sub> when DPM<sup>+</sup> formation is rate-controlling and in agreement with conclusions from previous studies. Whether benzyl alcohol undergoes a concerted dehydration during the C-C bond formation as proposed by Martinez-Espin et al. or dehydration to form a phenylmethelium cation surface species followed by C–C bond formation to form DPM<sup>+</sup>, as proposed

by Climent et al., <sup>9</sup> cannot be ascertained from the experimental data presented here because these steps are kinetically irrelevant.

The second kinetically relevant step in this reaction sequence is the benzene-catalyzed proton transfer from DPM<sup>+</sup> to the zeolite framework to desorb the final product, DPM. From isotopic switching experiments, we determined that the reaction order in HCHO decreased because the fractional coverage of DPM<sup>+</sup> approached unity, not because the fractional coverage of HCHO approached unity. This suggests that the denominator term in eq 12  $K_{\rm HCHO}P_{\rm HCHO,0}/(1 + K_{\rm hyd}P_{\rm H_2O})$ , which corresponds to the fractional coverage of HCHO, is negligible at the reaction conditions examined in this work. Parameter estimation results suggest that  $K_{\rm hyd}P_{\rm H_2O}$   $\gg 1$  and  $K_{\rm C_6H_6}P_{\rm C_6H_6} + K_{\rm H_2O}P_{\rm H_2O} \gg 1$ , such that the rate function for the formation of I\* (eq 10) is rewritten to eliminate all negligible terms as (eq 14)

$$\frac{r_{1}}{L} = \frac{\frac{k_{1}K_{\text{HCHO}}}{K_{\text{hyd}}K_{\text{H}_{2O}}} P_{\text{HCHO},0} P_{\text{C}_{6}\text{H}_{6}}}{\frac{K_{\text{C}_{6}\text{H}_{6}}}{K_{\text{H}_{2O}}} P_{\text{C}_{6}\text{H}_{6}} P_{\text{H}_{2O}} + P_{\text{H}_{2O}}^{2}} \theta_{*'} = \frac{\alpha P_{\text{HCHO},0} P_{\text{C}_{6}\text{H}_{6}}}{\beta P_{\text{C}_{6}\text{H}_{6}} P_{\text{H}_{2O}} + P_{\text{H}_{2O}}^{2}} \theta_{*'}$$

$$= f_{1}(P_{\text{HCHO},0}, P_{\text{C}_{6}\text{H}_{6}}, P_{\text{H}_{2O}}) \theta_{*'} \tag{14}$$

where  $\alpha$  and  $\beta$  are the lumped kinetic/thermodynamic parameters and  $\theta_{*'}$  is the fraction of sites without the adsorbed DPM<sup>+</sup>. The rate of consumption of DPM<sup>+</sup> is the rate of benzene-assisted proton transfer to the zeolite framework and is given by (eq 15)

$$r_2/L = k_2 P_{C_6 H_6} \theta_{DPM^+} = f_2 (P_{C_6 H_6}) \theta_{DPM^+}$$
 (15)

The steady-state rate is found by assuming  $d\theta_{\rm DPM^+}/dt = 0 = f_1\theta_{*'} - f_2\theta_{\rm DPM^+}$ , knowing that the fractional coverages sum to unity  $(\theta_{*'} + \theta_{\rm DPM^+} = 1)$ . From eqs 14 and 15, the steady-state rate of DPM formation is (eq. 16)

$$\frac{r_{\text{DPM}}}{L} = \frac{f_1 f_2}{f_1 + f_2} = \frac{\alpha k_2 P_{\text{HCHO},0} P_{\text{C}_6 \text{H}_6}}{\alpha P_{\text{HCHO},0} + \beta k_2 P_{\text{C}_6 \text{H}_6} P_{\text{H}_2 \text{O}} + k_2 P_{\text{H}_2 \text{O}}^2}$$
(16)

The kinetic parameters  $\alpha$ ,  $\beta$ , and  $k_2$  were estimated using Athena Visual Studio. The temperature dependence for each parameter was assumed to be of the Arrhenius form (eqs 17-19)

$$\alpha = \alpha_0 \exp\left(-\frac{E_{a,\alpha}}{R} \left(\frac{1}{T} - \frac{1}{363 \text{ K}}\right)\right) \tag{17}$$

$$\beta = \beta_0 \exp\left(-\frac{E_{a,\beta}}{R} \left(\frac{1}{T} - \frac{1}{363 \text{ K}}\right)\right)$$
 (18)

$$k_2 = k_{2,0} \exp\left(-\frac{E_{a,k_2}}{R} \left(\frac{1}{T} - \frac{1}{363 \text{ K}}\right)\right)$$
 (19)

where  $\alpha_0$ ,  $\beta_0$ , and  $k_{2,0}$  are the values of the kinetic parameters at 363 K. The results of the parameter estimation fits are summarized in Table 2. The fits to steady-state rates using the

Table 2. Parameters Estimated by Fitting the Model Rate Function (eq 16) to Steady-State Data

parameters	estimated values $\pm 95\%$ marginal HPD intervals
$\log_{10}(\alpha_0/\mathrm{s}^{-1})$	$-2.47 \pm 0.17$
$\log_{10}(eta_0)$	$0.33 \pm 0.32$
$\log_{10}(k_{2,0}/s^{-1} \text{ kPa}^{-1})$	$-3.41 \pm 0.16$
$E_{a,\alpha}$ (kJ mol <sup>-1</sup> )	79 ± 17
$E_{a,\beta}$ (kJ mol <sup>-1</sup> )	$51 \pm 32$
$E_{a,k_2}(kJ mol^{-1})$	$31 \pm 15$

parameters presented in Table 2 are shown in Figure 2 as solid curves for a subset of the data, and a parity plot on linear and log scales are given in Figure 6 for all of the experimental data.

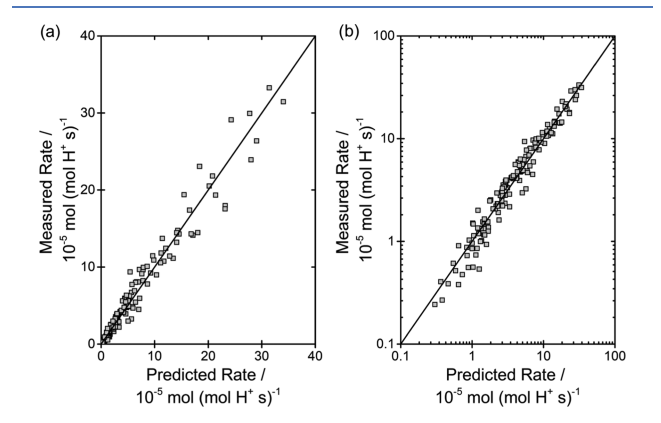


**Figure 6.** Measured versus predicted rate for all 153 rate measurements from 363 to 393 K, 0.005 to 0.35 kPa HCHO, 0.14 to 4.14 kPa  $C_6H_6$ , and 0.11 to 12.5 kPa  $H_2O$  on (a) a linear scale and (b) a log scale to better visualize low rate data.

All experimental conditions, measured rates, and predicted rates are tabulated in Table S1 of Section S6 of the Supporting Information. The six-parameter kinetic model (eq 16) derived based on the proposed reaction mechanism presented in Schemes 3 and 4 quantitatively captures the trends in the DPM formation rate with temperature and reactant partial pressures.

The model parameters in Table 2 were fit only to steadystate rate data, but also predicts the transients observed when starting the reaction from fresh catalyst or after step-changing the partial pressure of a reactant. The transient surface coverage of DPM<sup>+</sup> is found by solving the differential equation given in eq 20

$$\frac{\mathrm{d}\theta_{\mathrm{DPM}^{+}}}{\mathrm{d}t} = f_{1}(P_{\mathrm{HCHO},0}, P_{\mathrm{C}_{6}\mathrm{H}_{6}}, P_{\mathrm{H}_{2}\mathrm{O}})(1 - \theta_{\mathrm{DPM}^{+}}) 
- f_{2}(P_{\mathrm{C}_{6}\mathrm{H}_{6}})\theta_{\mathrm{DPM}^{+}}$$
(20)

The transient rate is solved piecewise from the start of one change in the reaction condition to the start of the next change in the reaction condition. Each time the reaction condition is changed, it is assumed that  $\theta_{\rm DPM^+}$  an infinitesimal time before the change is equal to  $\theta_{\rm DPM^+}$  an infinitesimal time after the

change. The solution to eq 15 with the initial condition  $\theta_{\text{DPM}^+}(t = t_0) = \theta_{\text{DPM}^+,0}$  is (eq 21)

$$\theta_{\text{DPM}^{+}}(t) = \frac{f_1}{f_1 + f_2} + \left(\theta_{\text{DPM}^{+},0} - \frac{f_1}{f_1 + f_2}\right)$$

$$\exp(-(f_1 + f_2)(t - t_0)) \ \forall \ t \in [t_0, t_1]$$
(21)

where  $f_1$  and  $f_2$  are the functions that appear in eqs 14 and 15,  $t_0$  is the time at the start of the current reaction condition, and  $t_1$  is the starting time for the next reaction condition. The transient rate is simply given by multiplying eq 21 by  $f_2$  (see eq 15), as shown by eq 22

$$\frac{r_{\text{DPM}}(t)}{L} = \frac{f_1 f_2}{f_1 + f_2} + \left( f_2 \theta_{\text{DPM}^+,0} - \frac{f_1 f_2}{f_1 + f_2} \right)$$

$$\exp(-(f_1 + f_2)(t - t_0)) \ \forall \ t \in [t_0, t_1]$$
(22)

Notice that the transient rate function (eq 22) requires only two additional parameters: the time since the previous change in reaction condition  $(t - t_0)$  and the DPM<sup>+</sup> coverage at the time of the change in reaction condition,  $heta_{ ext{DPM}^+,0}$ . The quantity  $heta_{ ext{DPM}^+,0}$  is zero if starting from fresh catalyst or the value of  $\theta_{\mathrm{DPM}^+}$  immediately before the step-change, found by evaluating eq 21 at  $t = t_1$  using the temperature and partial pressures from the previous condition. Thus, the transient can be modeled using the steady-state estimated parameters presented in Table 2. The model prediction for the transient rate (eq 22) when starting from a fresh catalyst and during the step-change in the partial pressure of each reactant is shown as solid curves in Figure 1. The model captures the time scales required to reach steady state and the behavior through the step-change in reactant partial pressures. The kinetic parameter derived from steady-state rate measurements accurately predicts the transient rates, exemplifying the connection between these phenomena and affirming the validity of the proposed reaction mechanism for DPM formation.

The model predicts the transient and steady-state reaction rates, and from eq 21, it can also predict the steady-state and transient fractional coverages of DPM<sup>+</sup>. The steady-state fractional coverage of DPM<sup>+</sup> was assessed at two reaction conditions using SSITKA (Figure 4). From eq 21, the steady-state fractional coverage of DPM<sup>+</sup> is  $\theta_{\text{DPM}^+}(t \to \infty) = f_1/(f_1 + f_2)$ . The predicted values for the steady-state coverages are in good agreement with the measured coverages, as shown in Table 3. Thus, the kinetic model quantitatively predicts

Table 3. Measured and Predicted Steady-State Fractional Coverages of  $\mathsf{DPM}^+$ 

Т (К)	P <sub>HCHO,0</sub> (kPa)	$P_{C_6H_6}$ (kPa)	$P_{C_6H_6}$ (kPa)	measured $Q_{\mathrm{DPM}^{^{+}}}$	$\underset{Q_{\mathrm{DPM}^{+}}}{predicted}$
393	0.020	0.40	4.0	0.18	0.14
393	0.20	0.40	2.0	0.68	0.82

transient rates, steady-state rates, and fractional coverages at a wide range of reaction conditions using only three fitted kinetic/thermodynamic parameters and three activation/thermodynamic energies.

#### 4. CONCLUSIONS

In this study, the mechanism of diphenylmethane (DPM) formation from HCHO and C<sub>6</sub>H<sub>6</sub> on SPP-HZSM-5 zeolite

catalysts in the presence of H<sub>2</sub>O cofeeds is determined by combining transient and steady-state rate measurements and isotopic switching experiments. Transients lasting several hours were observed during experiments starting from freshly regenerated catalysts and for each change in the reaction condition. These were determined to result from the slowly evolving fractional coverage of a surface intermediate with time on stream. The isotopologue distribution of DPM products after a switch from <sup>12</sup>C- to <sup>13</sup>C-labeled C<sub>6</sub>H<sub>6</sub> feed indicated that the surface intermediate has two six-membered rings and is likely a diphenylmethane benzenium ion (DPM<sup>+</sup>). The steady-state coverage of DPM+ was determined to vary significantly with reaction conditions, with increasing coverage corresponding to a shift in rate-controlling step from formation to the consumption of DPM<sup>+</sup>. Consumption of DPM<sup>+</sup> involves proton transfer from DPM+ to the zeolite framework. This proton transfer is mediated by the presence of aromatic species as evidenced by (i) the rate being discontinuous in time when the partial pressure of C<sub>6</sub>H<sub>6</sub> is step-changed, (ii) the steadystate rate of DPM formation being first-order in C<sub>6</sub>H<sub>6</sub> at high fractional coverages of DPM+, and (iii) DPM+ surface species persisting on the zeolite during a He flush until the introduction of toluene. A mechanism consistent with the observed trends in transient and steady-state reaction rates and the isotopic switching experiments was developed and a kinetic model based on this mechanism quantitatively captures all observations using three kinetic/thermodynamic parameters, each with an apparent activation energy to describe the temperature dependence.

# ■ ASSOCIATED CONTENT

# **Supporting Information**

The Supporting Information is available free of charge at https://pubs.acs.org/doi/10.1021/acscatal.0c02991.

Analysis of heat- and mass-transfer limitation during steady-state catalysis; degradation of SPP-HZSM-5 catalyst over repeated oxidative thermal treatments; temperature-programmed desorption of NH<sub>3</sub> and 2,6-di-tert-butylpyridine on SPP-HZSM-5; effect of 2,6-di-tert-butylpyridine on diphenylmethane formation rates; degree of rate control analysis for diphenylmethane formation rates during transients; table of diphenylmethane rate at all reaction conditions compared to model prediction; derivation of the DPM formation rate function at steady state (eq 12); discussion of the impact of transport effects on transient rate measurements; and analysis of benzaldehyde formation rates at steady state (PDF)

# AUTHOR INFORMATION

## **Corresponding Author**

Aditya Bhan — Department of Chemical Engineering and Materials Science, University of Minnesota—Twin Cities, Minneapolis, Minnesota 55455, United States; orcid.org/0000-0002-6069-7626; Email: abhan@umn.edu; Fax: (+1) 612-626-7246

### Author

Brandon L. Foley — Department of Chemical Engineering and Materials Science, University of Minnesota—Twin Cities, Minneapolis, Minnesota 55455, United States

Complete contact information is available at:

https://pubs.acs.org/10.1021/acscatal.0c02991

#### Notes

The authors declare no competing financial interest.

#### ACKNOWLEDGMENTS

We thank Dr. Dandan Xu for synthesizing the SPP-HZSM-5 catalyst, and B.L.F. thanks Dr. Thomas Chen, Professor Matthew Neurock, Dr. Andrew Hwang, Professor Praveen Bollini, Professor James Harris, Dr. Anurag Kumar, Dr. Linh Bui, Neil Razdan, Matthew Simons, Jacob Miller, Zhichen Shi, Dr. Sukaran Arora, and Dr. Udit Gupta for their helpful technical discussions. This material is based upon the work supported by the National Science Foundation Graduate Research Fellowship under Grant no. 00039202. We also acknowledge the National Science Foundation (CBET 1701534) for financial support.

#### REFERENCES

- (1) Hwang, A.; Kumar, M.; Rimer, J. D.; Bhan, A. Implications of Methanol Disproportionation on Catalyst Lifetime for Methanol-to-Olefins Conversion by HSSZ-13. *J. Catal.* **2017**, *346*, 154–160.
- (2) Hwang, A.; Bhan, A. Bifunctional Strategy Coupling  $Y_2O_3$ -Catalyzed Alkanal Decomposition with Methanol-to-Olefins Catalysis for Enhanced Lifetime. *ACS Catal.* **2017**, *7*, 4417–4422.
- (3) Martinez-Espin, J. S.; Mortén, M.; Janssens, T. V. W.; Svelle, S.; Beato, P.; Olsbye, U. New Insights into Catalyst Deactivation and Product Distribution of Zeolites in the Methanol-to-Hydrocarbons (MTH) Reaction with Methanol and Dimethyl Ether Feeds. *Catal. Sci. Technol.* **2017**, *7*, 2700–2716.
- (4) Müller, S.; Liu, Y.; Kirchberger, F. M.; Tonigold, M.; Sanchez-Sanchez, M.; Lercher, J. A. Hydrogen Transfer Pathways during Zeolite Catalyzed Methanol Conversion to Hydrocarbons. *J. Am. Chem. Soc.* **2016**, *138*, 15994–16003.
- (5) Arora, S. S.; Bhan, A. The Critical Role of Methanol Pressure in Controlling Its Transfer Dehydrogenation and the Corresponding Effect on Propylene-to-Ethylene Ratio during Methanol-to-Hydrocarbons Catalysis on H-ZSM-5. *J. Catal.* **2017**, *356*, 300–306.
- (6) Vasiliadou, E. S.; Gould, N. S.; Lobo, R. F. Zeolite-Catalyzed Formaldehyde–Propylene Prins Condensation. *ChemCatChem* **2017**, 9, 4417–4425.
- (7) Martinez-Espin, J. S.; De Wispelaere, K.; Westgård Erichsen, M.; Svelle, S.; Janssens, T. V. W.; Van Speybroeck, V.; Beato, P.; Olsbye, U. Benzene Co-Reaction with Methanol and Dimethyl Ether over Zeolite and Zeotype Catalysts: Evidence of Parallel Reaction Paths to Toluene and Diphenylmethane. *J. Catal.* **2017**, *349*, 136–148.
- (8) Hou, Z.; Okuhara, T. Catalytic Synthesis of Diphenylmethane from Benzene and Formalin with Water-Tolerant Solid Acids. *Appl. Catal., A* **2001**, *216*, 147–155.
- (9) Climent, M. J.; Corma, A.; García, H.; Primo, J. Zeolites in Organic Reactions. Condensation of Formaldehyde with Benzene in the Presence of HY Zeolites. *Appl. Catal.* **1989**, *51*, 113–125.
- (10) Zhang, X.; Liu, D.; Xu, D.; Asahina, S.; Cychosz, K. A.; Agrawal, K. V.; Al Wahedi, Y.; Bhan, A.; Al Hashimi, S.; Terasaki, O.; Thommes, M.; Tsapatsis, M. Synthesis of Self-Pillared Zeolite Nanosheets by Repetitive Branching. *Science* 2012, 336, 1684–1687. (11) Veefkind, V. A.; Lercher, J. A. On the Elementary Steps of Acid Zeolite Catalyzed Amination of Light Alcohols. *Appl. Catal., A* 1999, 181, 245–255.
- (12) Swindlehurst, G. R.; Kumar, P.; Xu, D.; Alhassan, S. M.; Mkhoyan, K. A.; Tsapatsis, M. Nucleation, Growth, and Robust Synthesis of SPP Zeolite: Effect of Ethanol, Sodium, and Potassium. *Top. Catal.* **2015**, *58*, 545–558.
- (13) Bates, S. A.; Delgass, W. N.; Ribeiro, F. H.; Miller, J. T.; Gounder, R. Methods for  $NH_3$  Titration of Brønsted Acid Sites in Cu-Zeolites That Catalyze the Selective Catalytic Reduction of  $NO_x$  with  $NH_3$ . J. Catal. 2014, 312, 26–36.

- (14) Bagnasco, G. Improving the Selectivity of NH3 TPD Measurements. J. Catal. 1996, 159, 249-252.
- (15) Khare, R.; Bhan, A. Mechanistic Studies of Methanol-to-Hydrocarbons Conversion on Diffusion-Free MFI Samples. *J. Catal.* **2015**, 329, 218–228.
- (16) Rybicki, M.; Sauer, J. Acidity of Two-Dimensional Zeolites. *Phys. Chem. Chem. Phys.* **2015**, *17*, 27873–27882.
- (17) Gounder, R.; Iglesia, E. The Catalytic Diversity of Zeolites: Confinement and Solvation Effects within Voids of Molecular Dimensions. *Chem. Commun.* **2013**, 49, 3491–3509.
- (18) Foley, B. L.; Bhan, A. Degrees of Rate Control at Non(Pseudo)Steady-State Conditions. ACS Catal. 2020, 2556–2564.
- (19) Bollini, P.; Chen, T. T.; Neurock, M.; Bhan, A. Mechanistic Role of Water in HSSZ-13 Catalyzed Methanol-to-Olefins Conversion. *Catal. Sci. Technol.* **2019**, *9*, 4374–4383.
- (20) Böhm, S.; Navrátil, R.; Kuthan, J. A Theoretical Study of the Methanediol Decomposition Mechanism. *J. Mol. Struct.* **1991**, 227, 277–283.
- (21) Iv, D. R. K.; Widicus, S. L.; Iii, W. A. G. A Theoretical Study of the Conversion of Gas Phase Methanediol to Formaldehyde. *J. Chem. Phys.* **2003**, *119*, 5117–5129.
- (22) Hazra, M. K.; Francisco, J. S.; Sinha, A. Gas Phase Hydrolysis of Formaldehyde to Form Methanediol: Impact of Formic Acid Catalysis. *J. Phys. Chem. A* **2013**, *117*, 11704–11710.
- (23) Kumar, M.; Anglada, J. M.; Francisco, J. S. Role of Proton Tunneling and Metal-Free Organocatalysis in the Decomposition of Methanediol: A Theoretical Study. *J. Phys. Chem. A* **2017**, *121*, 4318–4325.
- (24) Min, H. K.; Cha, S. H.; Hong, S. B. Mechanistic Insights into the Zeolite-Catalyzed Isomerization and Disproportionation of m-Xylene. *ACS Catal.* **2012**, *2*, 971–981.
- (25) Margarit, V. J.; Osman, M.; Al-Khattaf, S.; Martínez, C.; Boronat, M.; Corma, A. Control of the Reaction Mechanism of Alkylaromatics Transalkylation by Means of Molecular Confinement Effects Associated to Zeolite Channel Architecture. *ACS Catal.* **2019**, 9, 5935–5946.
- (26) Cha, S. H.; Hong, S. B. Reaction Intermediates and Mechanism of the Zeolite-Catalyzed Transalkylation of 1,2,4-Trimethylbenzene with Toluene. *J. Catal.* **2018**, 357, 1–11.
- (27) Svelle, S.; Olsbye, U.; Lillerud, K. P.; Kolboe, S.; Bjørgen, M. Diphenylmethane-Mediated Transmethylation of Methylbenzenes over H-Zeolites. *J. Am. Chem. Soc.* **2006**, *128*, 5618–5619.
- (28) Huang, J.; Jiang, Y.; Marthala, V. R. R.; Hunger, M. Insight into the Mechanisms of the Ethylbenzene Disproportionation: Transition State Shape Selectivity on Zeolites. *J. Am. Chem. Soc.* **2008**, *130*, 12642–12644.
- (29) Clark, L. A.; Sierka, M.; Sauer, J. Stable Mechanistically-Relevant Aromatic-Based Carbenium Ions in Zeolite Catalysts. *J. Am. Chem. Soc.* **2003**, *125*, 2136–2141.
- (30) Demuth, T.; Raybaud, P.; Lacombe, S.; Toulhoat, H. Effects of Zeolite Pore Sizes on the Mechanism and Selectivity of Xylene Disproportionation A DFT Study. *J. Catal.* **2004**, *222*, 323–337.
- (31) Clark, L. A.; Sierka, M.; Sauer, J. Computational Elucidation of the Transition State Shape Selectivity Phenomenon. *J. Am. Chem. Soc.* **2004**, *126*, 936–947.
- (32) Foley, B. L.; Bhan, A. Degree of Rate Control and De Donder Relations an Interpretation Based on Transition State Theory. *J. Catal.* **2020**, 384, 231–251.
- (33) Cortright, R. D.; Dumesic, J. A. Kinetics of Heterogeneous Catalytic Reactions: Analysis of Reaction Schemes. In *Advanced Catalysis*; Gates, B.; Knoezinger, H., Eds.; Academic Press: Cambridge, MA, 2001; Vol. 46, pp 161–264.
- (34) Bernasconi, C. F.; Wenzel, P. J.; Ragains, M. L. Proton Transfers in Aromatic and Antiaromatic Systems. How Aromatic or Antiaromatic Is the Transition State? An Ab Initio Study. *J. Am. Chem. Soc.* **2008**, *130*, 4934–4944.
- (35) Haw, J. F. Zeolite Acid Strength and Reaction Mechanisms in Catalysis. *Phys. Chem. Chem. Phys.* **2002**, *4*, 5431–5441.

- (36) Fang, H.; Zheng, A.; Xu, J.; Li, S.; Chu, Y.; Chen, L.; Deng, F. Theoretical Investigation of the Effects of the Zeolite Framework on the Stability of Carbenium Ions. *J. Phys. Chem. C* **2011**, *115*, 7429–7439.
- (37) Beck, L. W.; Xu, T.; Haw, J. F.; Nicholas, J. B. Kinetic NMR and Density Functional Study of Benzene H/D Exchange in Zeolites, the Most Simple Aromatic Substitution. *J. Am. Chem. Soc.* **1995**, *117*, 11594–11595.
- (38) Sreekumar, R.; Pillai, C. N. Reactions of Benzyl Alcohol and Dibenzyl Ether over Zeolites. *Catal. Lett.* **1993**, *19*, 281–291.